Spatiotemporal chaos stimulated by transverse Hopf instabilities in an optical bilayer system

P. V. Paulau, I. V. Babushkin, and N. A. Loiko*
Institute of Physics, Academy of Sciences of Belarus, Scaryna Prospekt 70, 220072 Minsk, Belarus
(Received 23 January 2004; published 29 October 2004)

We study two-dimensional spatiotemporal dynamics in an optical system of two identical nonlinear films irradiated from both sides by equal plane waves and show that a wide variety of chaotic behaviors can be obtained near the subcritical pitchfork bifurcation point. The regimes arising in the vicinity of asymmetrical steady state depend on stability of the symmetrical steady state at the same driving field, on interactions of Hopf and Turing instabilities occurring at the asymmetrical branch of solutions, and on a transverse wave number of the Hopf instability band center. The wave number is controlled by a phase shift of the field passed between two films, and the relative order of the Turing and Hopf bifurcations is controlled by a diffusion of charge carrier in a semiconductor media. Chaotic oscillating patterns are formed mainly by transverse Hopf modes rising due to a time delay in the system.

DOI: 10.1103/PhysRevE.70.046222 PACS number(s): 05.45.−a, 42.65.Sf, 42.60.Jf

I. INTRODUCTION

There are numerous works devoted to transverse pattern formation in nonlinear optical systems. Two generic types of bifurcations are responsible for static and dynamical patterns arising from a homogeneous steady state. Those are Turing and Hopf bifurcations, respectively. Simple periodic patterns, such as static hexagons, are formed due to the developing of several transverse static unstable modes inside the same instability band [1]. More complicated structures can be formed as a result of competition of modes inside two or more bands [2].

In turn, domains where oscillatory instabilities take place can be divided into homogeneous and space-periodic classes depending on which oscillating Fourier mode has a maximal gain: with zero or a finite wave number, correspondingly. Below, the latter case is referred to as a transverse Hopf instability band to distinguish it from the former homogeneous case (though the homogeneous Hopf band includes also modes with finite wave numbers but with lesser gain than the mode with zero wave number). An interaction of Hopf modes from different bands or with Turing modes strictly enlarges the list of possible behaviors. Traveling waves, drifting rhombus, and winking hexagons were observed as the result of resonant interaction under phase-matching conditions [3–6]. In the general case the interplay between Turing and Hopf modes can lead to more complex dynamics. Thus near a codimension-2 point where thresholds of Turing and homogeneous Hopf instabilities coincide ("codimension-2 Turing-Hopf bifurcation" in the terminology of Ref. [1]), different types of behaviors were obtained in addition to the existence of the pure modes [7–10]: bistability between the homogeneous Hopf branch of solutions and either pure Turing or Hopf-Turing mixed-mode branches and related localized structures; Turing-Hopf and subharmonic (resulting from self-induced subharmonic instabilities of the pure steady and Hopf modes) mixed modes that may become phase unstable giving rise to spatiotemporal chaos.

The purpose of the present paper is to analyze a competition between modes from the Turing and transverse Hopf instability bands, in contrast to Refs. [7–10]. As a paradigm, we consider an optical system consisting of two identical nonlinear thin films irradiated from both sides by equal plane waves. This system was introduced in Ref. [11] by Yu. A. Logvin and A. M. Samson. Such phenomena as optical bistability and symmetry breaking [12], static pattern formation [13], localized structures [14], homogeneous pulsing, and chaotic temporal regimes [11] were found. Here we focus mainly on the vicinity of pitchfork bifurcation, where the symmetrical steady state crosses the unsymmetrical branch. Both Turing and Hopf instabilities may coexist at the asymmetrical branch of solutions near this pitchfork bifurcations point if it is subcritical. The presence of several steady-state branches greatly increase the diversity of dynamics.

To control the system dynamics we change a coefficient of charge carrier diffusion in semiconductor media and a phase shift of field propagating through a linear medium between the films. It is shown that the phase shift controls the value of transverse wave numbers of unstable modes. Depending on it, instabilities with the smallest transverse wave numbers can arise via either Hopf or Turing bifurcation. The diffusion coefficient can be used to control the threshold of modulational instability changing the relative order between Turing and Hopf instabilities. Various behaviors including chaotic ones can be obtained near the codimension-2 bifurcation point. Among them there are regimes with spatial field distribution appearing as coexisting domains with different structures (for example, a vortex glass and "mosaiclike" patterns). Comparison of two cases when the Turing instability interacts with transverse or homogeneous Hopf instabilities is done. The influence of a stability of the symmetrical steady state coexisting with the asymmetrical one for taken parameters is elucidated.

II. BASIC EQUATIONS

The system under study consists of two nonlinear thin layers separated by a linear medium (Fig. 1). The nonlinear

*Fax: +375-172-393131;
email address: nloiko@dragon.bas-net.by

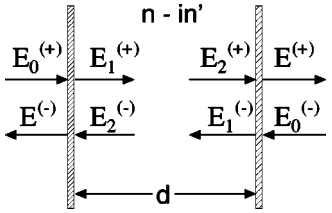

FIG. 1. The system consisting of two nonlinear films separated by absorbing medium with complex refraction index *n-in'*. *d* is the distance between the films, $E_0^{(+)}, E_0^{(-)}$ are slow complex amplitudes of fields incident into the system from the left and from the right, $E_1^{(+)}, E_1^{(-)}$ are ones transmitted through the films, and $E_2^{(-)}, E_2^{(+)}$ are the fields reaching the opposite film.

medium is considered in a two-level approximation. We suppose the polarization relaxation time is much shorter than other characteristic times in the system and adiabatically eliminates the polarization of the medium:

$$r_j = ie_j(n_j - 1)\Theta, \tag{1}$$

where r_j and e_j are the polarizations and fields normalized in accordance with Ref. [13], $j=1$ for the left and $j=2$ for the right film. $\Theta=(1+i\Delta)/(1+\Delta^2)$, n_j are normalized population differences, Δ is the frequency detuning between the incident field and the maximum of the absorption line normalized to the polarization relaxation rate.

In this approximation, the absorption line shape has Lorenz contour Θ, that often used for the description of resonant nonlinear media including semiconductors (see, for example, Ref. [15]). In the last case the interaction of light with the films is described by the equation [15]

$$\dot{n}_j = -n_j - \frac{|e_j|^2(n_j - 1)}{1 + \Delta^2} + D\Delta_\perp n_j. \tag{2}$$

Here, n_j are carrier densities normalized to their values at transparency, D is the correspondingly normalized carrier diffusion coefficient, $\Delta_\perp = \partial^2/\partial x^2 + \partial^2/\partial y^2$ is the Laplacian over transverse coordinates $\boldsymbol{r}_\perp = \{x, y\}$.

The field equations were obtained in Refs. [12,13] taking into account both propagation through the nonlinear thin films (the thickness of each layer is supposed much smaller than a wavelength of incident field) and through the linear gap between them, and have the following form:

$$\begin{cases} e_1(t) = e_{in1} - i\alpha r_1(t) - \rho e^{is} e^{-i\theta_\perp} i\alpha r_2(t - \tau), \\ e_2(t) = e_{in2} - i\alpha r_2(t) - \rho e^{is} e^{-i\theta_\perp} i\alpha r_1(t - \tau), \end{cases} \tag{3}$$

where ρ,, s, and τ stand, respectively, for losses, the phase shift, and a time delay due to propagation in the linear gap, k is the light wave number, $\theta=(d/k)\Delta_\perp$, and α describes the nonlinearity of the thin film [16],

$$\begin{cases} e_{in1} = e_0^{(+)}(t) + \rho e^{is} e^{-i\theta_\perp} e_0^{(-)}(t - \tau), \\ e_{in2} = e_0^{(-)}(t) + \rho e^{is} e^{-i\theta_\perp} e_0^{(+)}(t - \tau). \end{cases} \tag{4}$$

e_{in1}, e_{in2} are variables responsible for general contribution of fields incident on each layer from both sides. In the case of equal incident fields these variables are equal. Below we consider only this case. We assume also that the incident fields are spatially homogeneous and time independent.

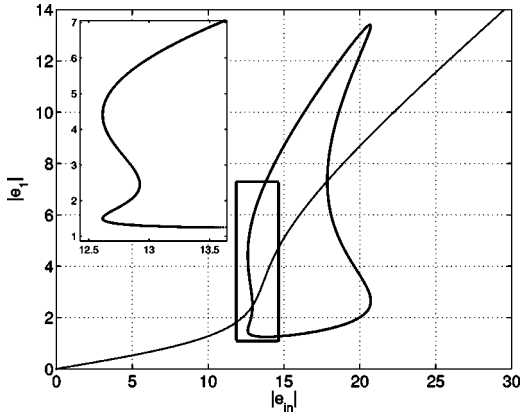

FIG. 2. Steady states of the system (2)–(4) for the following parameters: $\alpha=20.0, \Delta=2.0, \rho=0.5, s=0.9\pi$. The closed loop represents asymmetrical steady states ($e_1 \neq e_2$), whereas the open curve corresponds to symmetrical steady states ($e_1=e_2$). The region of interest is enclosed in the rectangle in the inset.

Beside the adiabatic elimination of polarization, the system (1)–(4) differs from ones considered earlier [12,13] by including the diffusion term in Eq. (2).

III. STEADY STATES AND LINEAR STABILITY ANALYSIS

In this section we consider the homogeneous steady states of the system (1)–(4). For this case, the carrier densities n_j can be expressed via the fields e_j and parameters of the system:

$$n_j = \frac{-1}{1 + \beta|e_j|^2} - 1, \tag{5}$$

where $\beta=1/(1+\Delta^2)$ At that, Eqs. (3) are reduced to

$$\begin{cases} e_1 = e_{in1} - \dfrac{\alpha\Theta e_1}{1 + \beta|e_1|^2} - \rho e^{is}\dfrac{\alpha\Theta e_2}{1 + \beta|e_2|^2}, \\ e_2 = e_{in2} - \dfrac{\alpha\Theta e_2}{1 + \beta|e_2|^2} - \rho e^{is}\dfrac{\alpha\Theta e_1}{1 + \beta|e_1|^2}. \end{cases} \tag{6}$$

Equations (6) can be written as a system of two cubic equations versus field variables. The solution of these equations for particular values of the parameters is presented in Fig. 2. A set of steady states is split into a symmetrical branch with $e_1=e_2$ which exists for all values of the incident field e_{in} and asymmetrical one corresponding to $e_1 \neq e_2$ [12]. We focus on the case when the pitchfork bifurcation is subcritical as shown in Fig. 2 that can be realized for large enough values of the nonlinearity parameter α.

Using the standard procedure of variation of the steady states, linearizing the system against variations (neglecting the terms of the second-order infinitesimal) and searching the solution of resulting system of differential equations in the form

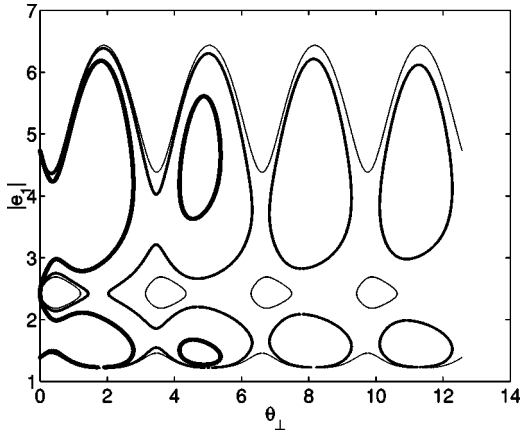

FIG. 3. Turing stability boundaries of the asymmetrical branch of the steady states enclosed in the rectangle in Fig. 2. The parameter values are as in Fig. 2. The thinnest line corresponds to the diffusion coefficient $D=0.0$, the line of the medium thickness to $D=0.1$ and the bold one to $D=0.5$.

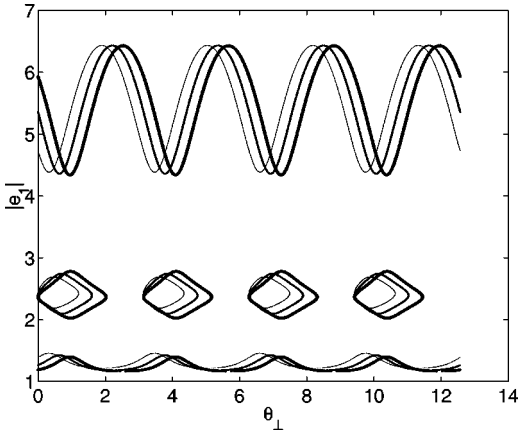

FIG. 4. Turing stability boundaries of the asymmetrical branch of the steady states (in the rectangle in Fig. 2) with changing the phase slippage. The thinnest line corresponds to $s=0.9\pi$, the line of the medium thickness to $s=0.8\pi$, and the thickest line to $s=0.7\pi$. $D=0.0$ and the other parameter values are as in Fig. 3.

$$\delta \boldsymbol{x}(\boldsymbol{r}_\perp, t) = \delta \boldsymbol{x}_0 e^{\lambda t + i \boldsymbol{k}_\perp \cdot \boldsymbol{r}_\perp} \tag{7}$$

[where $\delta \boldsymbol{x} = (\delta e_j, \delta e_j^*, \delta n_j)$ are small deviations of the variables from steady state, $j=1,2$] we obtain the characteristic quasipolynomial for determination of steady-states stability:

$$\sum_{j=0}^{2} P_j(\lambda, \boldsymbol{k}_\perp) e^{-2j\tau\lambda} = 0, \tag{8}$$

where $P_j(\lambda, \boldsymbol{k}_\perp)$ are polynomials of λ with coefficients depending on $\boldsymbol{k}_\perp$.

In Fig. 3, Turing stability boundaries [the condition $\lambda=0$ in Eq. (8)] for asymmetrical steady states are depicted. The thinnest line corresponds to the case of the absence of diffusion $D=0$, whereas the thickest one corresponds to the largest diffusion considered in this paper. It can be seen that the presence of diffusion leads to a decrease of the Turing unstable region. The transverse perturbations are damped more for larger values of the transverse wave number $k_\perp$. This action of the diffusion term is widely presented in the literature [2,3,17].

In Fig. 4, Turing stability boundaries for the same steady states as in Fig. 3 and $D=0$ are shown for different values of the phase shift s. The stability boundary for $s=0.9\pi$ is depicted by the thinnest line, and the decreasing of s is marked by the increasing of thickness. Therefore for this range of parameters, decreasing s leads to drift of the stability boundaries in the direction of large $k_\perp$ giving the way to control $k_\perp$ of the unstable mode.

For the sake of clarity, we depicted in Figs. 3 and 4 only changing of the Turing stability boundaries versus variation of the control parameters. However, if the pitchfork bifurcation is subcritical, Hopf instabilities can arise due to the time delay [13]. The Hopf bifurcation boundaries [obtained from the condition $\mathrm{Re}\,\lambda=0, \mathrm{Im}\,\lambda\neq 0$ in Eq. (8)] are depicted by thin lines in Fig. 5 and possess analogous properties. In this picture, static stability boundaries are also shown by thick lines. One can see that there are Hopf instability domains which are not included in the Turing instability regions.

In dependence on the phase slippage, the instability domain with smallest values of $k_\perp$ can be either a Turing or Hopf one. Below, we consider the latter case presented in Figs. 5 or 6(a)–6(c) and focus on the pair of Hopf and Turing bifurcations that occur first when the input field amplitude is decreased. At zero diffusion coefficient the upper threshold for Turing instability is higher than the Hopf bifurcation point, and the system demonstrates various static spatial structures [13]. By changing the diffusion coefficient, we can decrease the range of steady states unstable to transverse perturbations (both Hopf and Turing). The transverse instabilities are decreased more for larger values of the transverse wave number of corresponding transverse perturbations. We can therefore change the relative order between the two bifurcations as shown in Fig. 6. Similar changes of critical points of Turing and Hopf instabilities were obtained for reaction-diffusion models [7,8] and for an optical parametric oscillator [9,10].

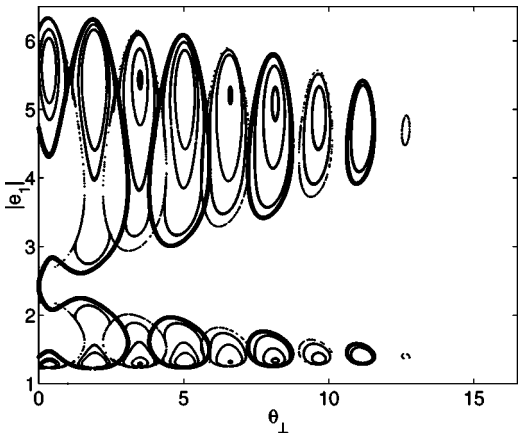

FIG. 5. Hopf and Turing stability boundaries for $D=0.25, \tau=5.0$, and the other parameter values as in Fig. 2. Hopf boundaries are marked by thin lines whereas Turing boundaries are marked by bold ones.

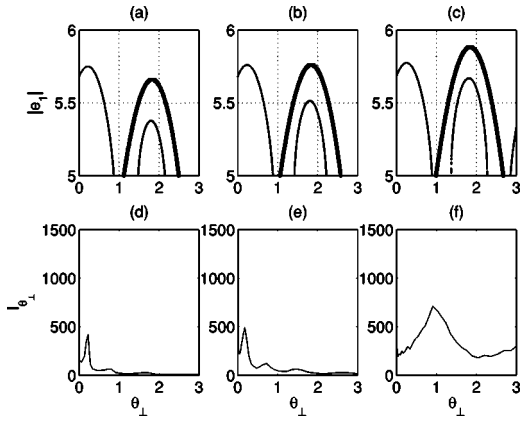

FIG. 6. (a), (b), (c) The field range in the left film near threshold of modulational instability and the parts of Hopf (left band) and Turing (right band) instability domains. (d), (e), (f) The azimuthally averaged spatial structure factor $I(\theta_\perp,t)$ corresponding to the far field presented in Figs. 9(a)–9(c). The parameters are $\alpha=18.0; D=0.5$ (a), (d), 0.35 (b), (e), 0,15 (c), (f); the other parameter values are as in Fig. 5.

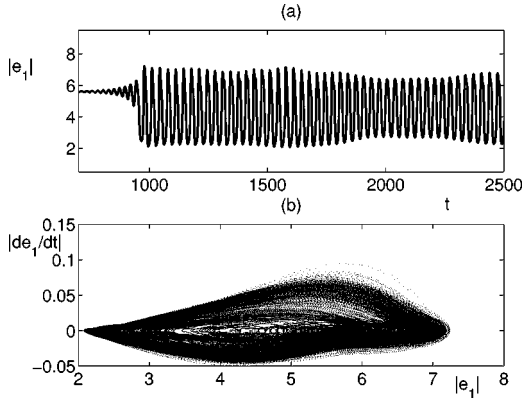

FIG. 7. (a) Dependence of the field in a single point of transverse section of the left film versus the time. (b) The corresponding trajectory in the phase space. The parameter values are as in Fig. 6(b), $e_{in}=10.88$, the initial value $e_1=5.6$.

It is worth noting a difference between the two cases presented in Figs. 5 and 6. For $\alpha=20$ (Fig. 5), the unstable part of the asymmetrical steady-state branch coexists with stable symmetrical states. This case is realized when the upper bifurcation point of the first instability band of the asymmetrical state is below the pitchfork bifurcation point. If the nonlinearity parameter is decreased as for Fig. 6, the asymmetrical branch changes its shape by such a way that the top of the first unstable band of asymmetrical states coexists with the unstable symmetrical branch. We show below that the stability of symmetrical steady states strongly influences the system behavior originating from an unstable asymmetrical steady state.

IV. NUMERICAL SIMULATIONS

In this section, we consider the spatiotemporal regimes obtained in the system under consideration. In numerical simulations, the split-step method has been used with fast Fourier transform on every step of integration that implies periodic boundary conditions. The grid size 128×128 was used. An asymmetrical steady state is taken as the initial condition for further simulations with small spatial noise added. Evidently, this precision is enough for regimes when only Hopf modes are active with comparatively small wave numbers as in Figs. 9(a), 9(b), and 9(d). Numerical integration of the system with parameters of Figs. 8(c) and 10 have been fulfilled also with higher precision using a 256×256 grid, that have confirmed the obtained results.

As shown in the previous section, by changing the diffusion coefficient D we can obtain codimension-2 bifurcation point where thresholds of Turing and transverse Hopf instabilities coincide [Fig. 6(b)]. For those parameters and the operating point situated slightly below the instability threshold, the system tends to the unstable homogeneous steady state at first, but then begins to withdraw from it. The field evolution after that transient stage is shown in Fig. 7(a). The behavior consists of fast, almost periodic, temporal oscillations with a low frequency chaotic envelope. The frequency of fast variations in Fig. 7(a) is close to the Hopf frequency at the boundary of the unstable band in Fig. 6(b). The phase portrait of the regime for a single point of the transverse plane is presented in Fig. 7(b). The chaotic "mosaiclike" spatial field distribution shown in Fig. 8(a) is formed. However, this state is not ultimate. There are self-organization processes in the system: in the long run, rotating spirals are spontaneously nucleated in the transverse plane and grow until a certain domain of the entire space is filled. The dynamics of the remaining part is held as before. The evolution of the spiral part is similar to the transition from a turbulent regime to a vortex glass [18]. The snapshot of transverse distribution of the field at this stage is shown in Fig. 8(b). In domains filled with spirals the time envelope becomes more smooth and the spatial picture is more ordered. Nevertheless, this regime remains slightly chaotic during all times of calculation.

The far field evolution of the above described dynamics is the following. When the system goes away from the unstable steady state, a ring of Fourier harmonics is excited with wave numbers close to the wave number of the transverse Hopf

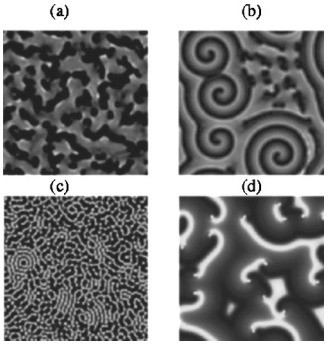

FIG. 8. Snapshots of the field in the left film. (a), (b) $e_{in}=10.88$, the initial value $e_1=5.6: t=1500$ (a), $t=40\,000$ (b); (c) $D=0.15, e_{in}=10.89$, the initial value $e_1=5.7, t>20\,000$; (d) $D=0.29$, $s=\pi, e_{in}=12.36$, the initial value $e_1=5.7, t=20\,000$; the other parameter values are as in Fig. 7.

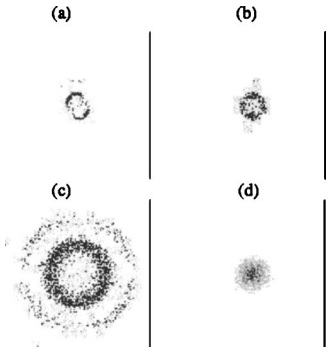

FIG. 9. Transverse far-field distribution for $D=0.5$ (a), 0.35 (b), 0,15 (c), 0.29 (d); $s=0.9\pi$ (a)–(c), π (d); the other parameter values are as in Fig. 6 and $t=40\,000$ (a), (b), 20 000 (c), (d).

mode. During the mosaiclike period [Fig. 8(a)] the ring evolves to a disc shape. Near and far fields at this stage of evolution are similar to that predicted for a CO_2 laser with saturable absorber operating far from the laser threshold [19]. On the last stage, the ring becomes again more visible though the mode excitement is not uniform along the ring [Fig. 9(b)].

It is worth noting that the modulus of space Fourier transform of the field e_1 used for calculation of the far field in a certain moment of time could be used to determine the structure factor [20,21]. This technique is useful for characterization of spatial and temporal scales and correlations of a chaotic state. To compare numerical results with stability analysis, we determine here only an instantaneous azimuthally averaged spatial structure factor $I(k_\perp,t)$ [21]. This factor for Fig. 8(a) clearly indicates that only transverse Hopf instability band is involved into dynamics of vortexes coexisting with the mosaiclike turbulence [compare Figs. 6(b) and 6(e)]. The field behavior in the second layer is similar but has another amplitude of oscillations (asymmetrical regime).

If the system operates closer to the maximum of the transverse Hopf instability band in Fig. 6(b), then the traveling rolls are formed. The time of their formation is comparatively short. The field evolution is approximately the same as in the previous case. Chaotic motion is produced evidently by defects, the number of which is reduced with time. Similar behaviors were observed also in the whole range of field amplitudes presented in Fig. 6(a) for a larger value of the diffusion coefficient when the critical point of transverse Hopf instability is higher than the Turing bifurcation point. Those structures are created mainly by transverse Hopf modes as shown in Figs. 6(d) and 9(a). In comparison with Fig. 9(b), only two segments of the ring are excited giving evidence of a dynamically induced anisotropy in the system.

If the diffusion is reduced so that the Turing critical point is the first to be observed at decreasing the input field [Fig. 6(c)], obtained spatial structures are approximately stationary (the amplitude of temporal pulsations $\simeq 10^{-4}$) and resemble disordered spaced defect chains or clusters typical for an isotropic system [1] [Fig. 8(c)]. At that, a ring of Fourier modes is excited again [Fig. 9(c)], but its characteristic wave number is between centers of the Hopf and Turing instability bands [Fig. 6(f)]. The ring is comparatively wide and occupies a part of both bands. Those features indicate a formation of mixed modes like that obtained near a codimensional-2 point in the case of the homogeneous Hopf instability band [1,7–10]. There is also the second weak ring with a double wave number in Fig. 9(c).

To compare both cases of the instability interactions involving the homogeneous or transverse Hopf instability in more detail, we change the phase slippage s and hence shift the domain of instability in respect to $k_\perp$ keeping the condition for occurrence of the codimensional-2 point by changing diffusion D. Thus for $s=\pi$ the system is dynamically unstable in respect to perturbations with $k_\perp$ belonging to a narrow band centered at $k_\perp=0$ (the homogeneous Hopf instability band). Near the instability threshold we have observed that the zero Fourier harmonic plays the main role in dynamics and a limit cycle is developed with a very weak long-wavelength spatial modulations. The limit cycle is a symmetrical state ($e_1=e_2$) in contrast with the regimes described above. When the operating point is shifted more from the threshold, this state loses stability keeping the symmetry and a new complex spatiotemporal behavior is observed after a long transient period. Its evolution in time consists of fast and slow oscillations as presented in Fig. 7; the spatial distribution shown in Fig. 8(d) is characterized by moving bright separate curves on the almost homogeneous background. The main active part in the space spectrum is condensed near zero wave number [Fig. 9(d)].

It is worthwhile to remind one that the above scenarios have been obtained when a top of the Hopf instability domain corresponds to a value of incident field higher than the pitchfork bifurcation point, so the homogeneous symmetrical state existing at this e_{in} is unstable. In the opposite case which is realized for higher values of the nonlinearity parameter α as in Fig. 2, perfect rotating spirals have been obtained instead of rolls near the maximum of the transverse Hopf instability band when it is higher than the maximum of the Turing band. Obtained numerical results demonstrate that starting from the unstable asymmetrical steady state, the field at a considerable part of the transverse section tends to the stable homogeneous symmetrical state. The remaining pieces of the spatial field distribution are kept asymmetrical and evolve to bright curves that are then transformed into rotating spirals. From a certain moment of time, each of the spirals occupies a constant domain. The time evolution of the field in a single point of the transverse cross section is a limit cycle with the frequency close to the Hopf one. However, with the decrease of the incident field, this regime becomes unstable and spirals untwist into traveling rolls as in the case $\alpha=18$.

The field distribution near a codimension-2 point for $\alpha=20$ also differs from that presented in Fig. 8(b), though temporal oscillations of a single point are similar. Instead of vortexes coexisting with chaotic domains, narrow traveling stripes coexisting with small domains of more complex behavior and with almost homogeneous domains are observed [Fig. 10(a)]. Correspondingly, two directions of wave vectors can be distinguished in the far field [Fig. 10(c)]. Besides, there are space harmonics close to zero wave number that are evidently responsible for long-wavelength perturbations of the background.

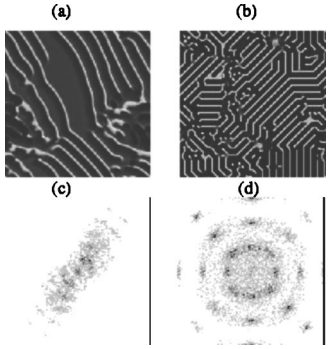

FIG. 10. Snapshots of the near (a), (b) and far (c), (d) fields in the left film. (a), (c) $D=0.29, e_{in}=11.57$, the initial value $e_1=6.21, t=20\,000$; (b), (d) $D=0.25, e_{in}=11.59$, the initial value $e_1=6.25, t>20\,000$; the other parameter values are as in Fig. 5.

The almost stationary space distributions for this value of α and smaller diffusion [Fig. 10(b)] is determined mainly by two rings as for $\alpha=18$ [Figs. 8(c) and 9(c)]. But in contrast with that case, only eight spots on every ring in the far field are excited [Fig. 10(d)]. As a result, the structure in Fig. 10(b) looks more regular than in Fig. 8(c). It includes comparatively large domains with rolls the incline of which is changed from one domain to another.

When the Turing instability band competes with the homogeneous Hopf instability band ($s=\pi$) for $\alpha=20$ a symmetrical homogeneous cycle ($e_1=e_2$) is observed near the codimension-2 point. This cycle loses stability with the decreasing of the incident field and the system settles down on the stable homogeneous symmetrical steady state.

V. DISCUSSION AND CONCLUSION

It is known that chaotic modulations of much faster periodical regime are encountered in time-delay optical systems, both spatiotemporal [22] and purely temporal [23,24] rather than in mean-field models. One of the reasons is that Hopf instability bands disappear for small delay. Another one is that a time-delay system is effectively infinite dimensional, which gives a possibility for chaotic behavior.

In this work, we have considered the system of two nonlinear thin films, separated by a linear medium. The delay in the system is caused by a time passage of the field between the layers. We focus on the case when the fields incident from both sides on the system are equal. Nevertheless, for certain parameters the system can have along with symmetrical homogeneous steady states ($e_1=e_2$) asymmetrical ones arising due to a pitchfork bifurcation (Fig. 2). We have demonstrated that this region is rich in respect to different instabilities if the pitchfork bifurcation is subcritical. The delay causes Hopf instabilities at the asymmetrical branch of solutions besides the Turing instability existing at zero delay. A Hopf bifurcation occurs with zero or a finite transverse number depending on the phase slippage between the films. Relative order of the Hopf and Turing bifurcations is driven by diffusion in a nonlinear media. A variety of spatiotemporal behaviors have been observed that could be classified by the next manner:

I. Interplay between the Turing and transverse Hopf instabilities results only in asymmetrical behaviors.

A. Region of parameters where unstable homogeneous asymmetrical steady states coexist with unstable symmetrical states ($\alpha=18$).

(1) Hopf modes are dominant: traveling rolls with defects. As known, defects often arise from long-wavelength disturbances [1,25,26].

(2) Codimension-2 point: (i) traveling rolls near the critical point; (ii) transition with decrease of the incident field to the defect mediated turbulence coexisting in two configurations, a vortex glass and mosaiclike patterns. This state is similar to the coexisting of a vortex glass and vortex liquid obtained in Ref. [27].

(3) Turing modes are dominant: almost stationary clusters of defects.

B. Region of parameters where unstable homogeneous asymmetrical steady states coexist with stable symmetrical states ($\alpha=20$).

(1) Hopf modes are dominant: (i) perfect vortex near the critical point and (ii) traveling rolls far from it.

(2) Codimension-2 point: coexisting of traveling stripes with chaotic and homogeneous domains.

(3) Turing modes are dominant: domains with almost stationary reoriented oblique rolls with boundaries of a "zigzag" type or destroyed by point defects.

II. When the interplay between the Turing and homogeneous Hopf instability takes place, only symmetrical behaviors have been observed for the case of codimension-2 point: homogeneous limit cycle near the critical point; chaotic moving bright curves on the homogeneous background (at $\alpha=18$) or the homogeneous steady states (at $\alpha=20$) far from the bifurcation.

So, behavior of the considered system depends not only on the interaction of Turing and Hopf instabilities of asymmetrical steady states, but also on a type of the Hopf bifurcation (homogeneous or space-periodic) at the center of the instability band and the stability of homogeneous symmetrical steady states existing at taken parameters. Potentialities to change those characteristics open opportunities to drive the system behavior from a homogeneous state to turbulence with different space structures. A better understanding of processes occurring in the system along with changes of the parameters could be achieved by a weak nonlinear analysis. However, that task presents a separate difficult problem since consideration of two coupled complex Swift-Hohenberg equations for fields in each layer is necessary. Moreover, taking into account that the carrier relaxation time is comparable with the time delay for the present parameters, those equations must be coupled to a mean flow as it takes place for a class B laser [28]. Such investigations are planned in the near future.

[1] D. Walgraef, *Spatio-Temporal Pattern Formation* (Springer-Verlag, New York, 1996).
[2] E. V. Degtiarev and M. A. Vorontsov, J. Mod. Opt. **43**, 93 (1996).
[3] S. L. Lachinova and W. Lu, J. Opt. B: Quantum Semiclassical Opt. **2**, 393 (2000).
[4] N. A. Loiko and Yu. A. Logvin, Laser Phys. **8**, 322 (1998).
[5] Yu. A. Logvin, B. A. Samson, A. A. Afanas'ev, A. M. Samson, and N. A. Loiko, Phys. Rev. E **54**, R4548 (1996).
[6] Yu. A. Logvin and N. A. Loiko, Phys. Rev. E **56**, 3803 (1997).
[7] M. Meixner, S. Bose, and E. Schol, Physica D **109**, 128 (1997).
[8] A. De Wit, D. Lima, G. Dewel, and P. Borckmans, Phys. Rev. E **54**, 261 (1996).
[9] M. Tlidi, P. Mandel, and M. Haelterman, Phys. Rev. E **56**, 6524 (1997).
[10] M. Tlidi and P. Mandel, Phys. Rev. A **59**, R2575 (1999).
[11] Yu. A. Logvin and A. M. Samson, Zh. Eksp. Teor. Fiz. **102**, 472 (1992) [Sov. Phys. JETP **75**, 250 (1992)].
[12] I. V. Babushkin, Yu. A. Logvin, and N. A. Loiko, Quantum Electron. **90**, 133 (2000).
[13] I. V. Babushkin, Yu. A. Logvin, and N. A. Loiko, Zh. Eksp. Teor. Fiz. **117**, 149 (2000) [JETP **90**, 133 (2000)].
[14] I. V. Babushkin, Yu. A. Logvin, and N. A. Loiko, J. Opt. B: Quantum Semiclassical Opt. **2**, L15 (2000).
[15] T. Maggipinto, M. Brambilla, and W. J. Firth, IEEE J. Quantum Electron. **39**, 206 (2003).
[16] M. G. Benedict, V. A. Malyshev, E. D. Trifonov, and A. I. Zaitsev, Phys. Rev. A **43**, 3845 (1991).
[17] E. Grosse Westhoff, V. Kneisel, Yu. A. Logvin, T. Ackemann, and W. Lange, J. Opt. B: Quantum Semiclassical Opt. **2**, 386–392 (2000).
[18] I. S. Aranson and L. Kramer, Rev. Mod. Phys. **74**, 99 (2002).
[19] A. Barsella, C. Lepers, M. Taki, and P. Glorieux, J. Opt. B: Quantum Semiclassical Opt. **1**, 64 (1999).
[20] Hao-wen Xi, Xiao-jun Li, and J. D. Gunton, Phys. Rev. Lett. **78**, 1046 (1997).
[21] S. W. Morris, E. Bodenschatz, D. S. Cannell, and G. Ahlers, Physica D **97**, 164 (1996).
[22] M. Le Berre, A. S. Patrascu, E. Ressayre, and A. Tallet, Phys. Rev. A **56**, 3150 (1997).
[23] D. Lenstra and M. Yousefi, in *Fundamental Issues of Nonlinear Laser Dynamics*, edited by B. Krduskopf and D. Lenstra, AIP Conf. Proc. No. 548 (AIP, Melville, NY, 2000), p. 87.
[24] N. A. Loiko and A. M. Samson, Quantum Electron. **24**, 657 (1994).
[25] M. C. Cross and P. C. Hohenberg, Rev. Mod. Phys. **65**, 851 (1993).
[26] H. Sakaguchi, Prog. Theor. Phys. **84**, 792 (1990).
[27] C. Brito, I. S. Aranson, and H. Chate, Phys. Rev. Lett. **90**, 068301 (2003).
[28] J. Lega, J. V. Moloney, and A. C. Newell, Physica D **83**, 478 (1995).